LUND
UNIVERSITY

Selective Electron Extraction in Nanowire-based Solar Cells

Thesis submitted for the degree of BACHELOR of SCIENCE

Department of Physics

Division of Mathematical Physics

Supervisors:

Andreas Wacker

Alex Kalaee

Author:

Klára Nováková

Spring term 2019

Abstract

The transmission function for a three and four rectangular barrier system of InP and InAs is computed using the transfer-matrix method and the transmission formalism. The widths of the wells and the barriers are varied while the barrier height is kept constant. Such a multi-barrier structure is designed in order to act as a filter in a nanowire based solar cell, where effective hot carrier transport would lead to an increase in the efficiency of the current generation. In this case, the filter is designed in order to maximise the transmission in the range 0.492 eV $< E <$ 0.504 eV and minimise the transmission above 0.550 eV and below 0.460 eV. The optimal transmission for the three barrier filter was obtained for a structure with 6.8 nm wide potential wells, 1 nm wide outer barriers and 4 nm wide central barrier. On the other hand, the four barrier filter had the most satisfying results for potential wells of the widths 6.3, 6.3 and 6.8 nm and barriers of the widths 1, 1, 4 and 1.4 nm.

Acknowledgements

I would like to express my deep gratitude to both of my supervisors, Andreas Wacker and Alex Kalaee for their guidance and support throughout the project. Without their useful comments and constructive feedback, this thesis certainly would have not been completed.

Moreover, I would like to thank all members of the division group of Nonequilibrium Quantum Transport in Nanosystems for their inspirational presentations of their work which deepened my understanding of the ongoing research. Lastly, I would like to thank Maitane Muñoz Basagoiti and André Nüßlein for their comments on language and layout matters.

Abbreviations

SE	Schrödinger equation
InAs	Indium arsenide
InP	Indium phosphide

Contents

1 Introduction

The conversion between light and electrical energy has been studied ever since the first observation of the photovoltaic effect in 1839 by Edmond Becquerel, the father of the 1903 Nobel laureate in Physics Henri Becquerel. The photovolatic effect describes the generation of electric current and voltage of an illuminated material. When light, in the form of photons, is absorbed by the material, its electrons get excited to higher energy states. One of the greatest applications of the photovoltaic effect are solar cells which directly convert light into electrical energy via the mechanism of charge separation. One can classify solar cells based on the way they separate charge. The most common solar cells are the p-n junction cells which separate the charge using an electric field. Such cells will now be discussed in greater detail.

When a solar cell is in the dark, its current-voltage (I-V) characteristic is identical to the one of a diode; a large current is observed when the forward bias is applied while in the case of the reverse bias, only very insignificant amount of current flows through. Conversely, when a solar cell is illuminated, the I-V curve is shifted in the direction of the negative current I by an amount I_L as shown in Fig. 1. When the voltage across the solar cell is zero, the current is at its maximum possible value, I_{sc}. On the other hand a maximum voltage, known as the open circuit voltage V_{oc}, is measured when no current flows through the cell. The aim is to achieve the highest possible power output P, where $P = IV$. The I-V plot is a very useful tool for this task, as one can find the optimal operation values of the current and voltage, I_{mp} and V_{mp}, of the cell yielding the desired maximal power output as illustrated in Fig. 1 by the dashed rectangle.

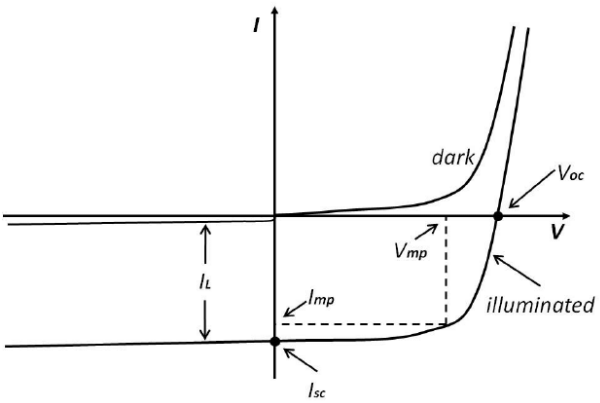

Figure 1: The I-V characteristic of a solar cell, figure taken from Ref. [3].

Let us now consider the illumination and the processes that follow more thoroughly. A solar cell absorbs light energy in the form of photons. The absorbed photons excite the electrons from the valence band to the conduction band and thus create electron-hole pairs. If an electron-hole pair is created in the depletion zone of the p-n junction, the electric field pulls the electrons and holes towards contacts on opposite sides of the cell. The electrons are accelerated towards the n-side and the holes to the p-side, as shown in Fig. 2. Thereby a photocurrent, I_{photo}, of the respective charge carriers is generated through the device and hence a potential difference, V, between the metal contacts on each side of the cell is created. The photocurrent is reduced by the diffusion current, $I_{diffusion}$, of the majority carriers, which is increased as the bias across the junction is increased. Therefore, as mentioned earlier, the selection of the operation variables of the solar cell is crucial. The potential difference across the device is then used to drive a current through an external load of a certain resistance.

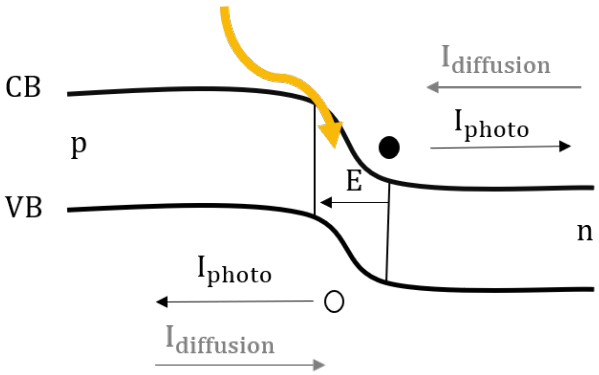

Figure 2: A scheme of the p-n junction in a solar cell, where E is the electric field created in the depletion zone and the incoming photon is indicated by the yellow arrow.

The currently most widely used single junction semiconductor solar cells, such as mono-crystalline and thin film cells, shown in Fig. 3, have a limited efficiency with its highest theoretical value of 30 % given by the Shockley-Queisser limit, Ref. [2]. One of the factors that prevents researchers from reaching this value is the recombination of the carriers resulting from a short lifetime of the minority carrier in the electron-hole pair. This stems from the fact that the minority carrier has a very high chance to recombine with the majority carrier on the side of the junction that it is being pulled towards. Such a recombination can have various resulting effects. It can lead to the emission of a photon (radiative) or the energy from the recombination can be absorbed by another

electron (Auger process). Alternatively, it can undergo recombination processes including surface and grain boundary recombination or it can interact with traps and recombination centres. Such recombination processes can be reduced by improving the engineering of the cell by optimising the contacts, introducing a potential barrier at the back of the cell (which reflects electrons and reduces rear surface recombination) or by utilising a material of higher quality. Other parameters that affect the efficiency include the reflectivity of the front surface and the directivity of the band gap of the material used. Ref. [2]

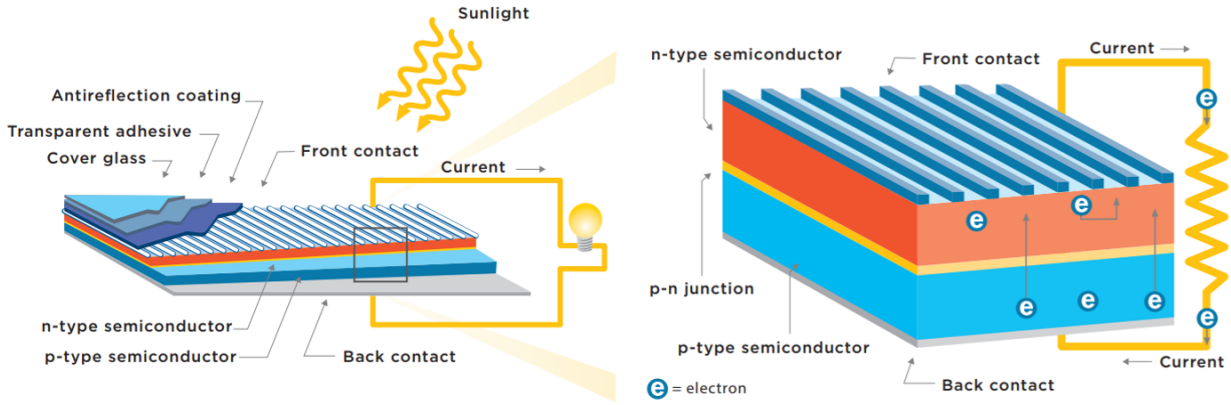

Figure 3: The currently most widely used solar cells, the thin film cell (on the left) and a silicon mono-crystalline cell (on the right), are depicted above, figure taken from Ref. [4].

Many researches focus on improving such single junction cells in order to reach as close as possible to the 30 % efficiency limit outside of the laboratory (See Ref. [1]). Others concentrate on finding new materials with better absorption quality or look for inspiration in nature with the aim of reproducing the mechanism of photosynthesis used by plants with almost 100 % efficient conversion rate of solar energy (See Ref. [1]). However, these are not the only solutions to the efficiency question. The alternative path that can be taken is to increase the limiting 30% efficiency value itself.

First, let us consider the features that restrict the efficiency of a single junction semiconductor cell as quantified by the Shockley-Queisser limit. Single junction solar cells can only be fully efficient for absorbing a small range of the solar spectrum when the photon energy is equal to the size of the band gap of the material the cell is made out of. Since the range of photons absorbed is limited by the band gap size, photons of energy lower than the band gap are not absorbed at all, while photons with higher energy are not ab-

sorbed efficiently. When a highly energetic photon is absorbed by the cell, it gives rise to an electron with high amount of kinetic energy which cannot contribute to the electricity generation. This is due the fact that the high energetic electron, referred to as a "hot electron", quickly thermalises by emitting phonons which in turn heat up the cell and hence dissipate the energy. Another factor that limits the efficiency of the solar cell is that each photon only generates one electron-hole pair that can contribute to the energy generation.

One possible solution that combines all three aspects is the nanowire-based solar cell design which shall be the starting point for this thesis. A nanowire-based solar cell is a type of an intermediate band cell which consists of a multi-level system, in this case realised by a multi-barrier system created by alternating layers of semiconducting materials with very different band gap size, Indium Arsenide (InAs) and Indium Phosphide (InP) in the case of this thesis, as depicted in Fig. 4. In this way the cell can absorb photons of a

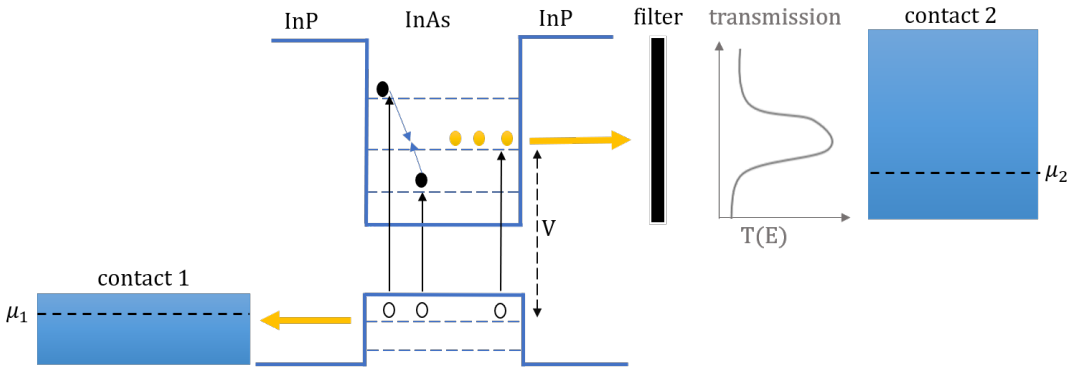

Figure 4: The principle of hot carrier transport, where the desired transmission function $T(E)$ is displayed.

broad range of energies and simultaneously efficiently deal with the "hot" carriers. It does so by harnessing some of the excess kinetic energy from photogenerated "hot" carriers, which reside on the upper levels, before they "cool down". The carriers transfer some of their kinetic energy to generate more electron-hole pairs as they de-excite by the process of impact ionisation and thus increase the current produced. However, for the impact ionisation between the electrons to occur, the electrons from the higher energetic levels must be prevented from tunnelling through the barrier system. On the other hand, if the electrons that populate the low energy levels (lower than the chemical potential μ_2 of the contact on the other side of the barrier system) tunnel through they can be re-emitted by the contact, resulting in a current flow against the photocurrent. Thus only electrons

of a specific range of energies shall be extracted for the current generation to be efficient. Such electron extraction can be done utilising an energy filter realised by a multi-barrier system. The aim of this thesis will be the design of such a filter, which shall be based on barrier systems consisting of three and four barriers as larger systems would make the practical engineering rather complicated.

In the first part of this thesis, the parameters of the device are introduced. Later, the different aspects of electron transport in heterostructures, necessary for the computation of the transmission and the later analysis of the results, are summarised. A brief discussion of the transmission formalism is included in this part as well in order to give more context and justification for the computation of the transmission function. In the second part, the results for a three and a four barrier filter are discussed and lastly a short summary concluding the results is given.

2 Filter Parameters

The multi-barrier system is formed by repeated layers of InAs and InP which have quite different band gaps (See Ref. [5] for exact values) meeting the first criteria for making a heterostructure. The second condition for materials to form a heterostructure is the almost identical value of the lattice constant. In the case of a bulk crystal structure, a lattice constant mismatch leads to a deformation of the crystals. In order for such a structure to exist, substantial amounts of pressure would be required. It is therefore impossible to grow materials with a lattice constant mismatch under standard conditions in this way. However, this is not the case on the nanoscale. Nanowires enable materials with different lattice constants to be grown on top of each other since the mismatch of lattice constants is compensated by the possible deformation of the structure, i.e. some parts of the nanowire being wider.

InP having a larger band gap forms the potential barriers in the conduction and valence band regions. However, in this thesis only the barrier system in the conduction band is considered as the valance band is more complicated due to the degeneracy of states. The difference between the band gaps of InAs and InP according to Ref. [6] yields a

conduction band offset larger than 0.6 eV which is around 60% of the band gap difference. The value used in the nanowire model is 0.7 eV and thus the height of the barriers of the filter is considered to be 0.7 eV in this thesis as well. The effective electron masses of InAs and InP used are

$$m(\text{InAs}) = 0.026 \cdot m_e \quad \text{and} \quad m(\text{InP}) = 0.0795 \cdot m_e$$

according to Ref. [5]. The desired filter should block electrons of energies above 0.550 eV and below 0.460 eV while maximising the transmission of electrons in the range 0.492 - 0.504 eV which corresponds to the central energy states of the nanowire heterostructure.

3 Transmission in Heterostructures

In this section, firstly the wavefunction that will describe the electron states in a nanowire will be assigned, later the theory behind resonant tunnelling shall be explained and a brief discussion describing the electron transport by means of the transmission formalism will be included. Moreover, the transfer matrix method for the calculation of the transmission function will be detailed. Lastly, the coefficients Ω and Γ, which later allow the analysis of the results, will be introduced.

3.1 The Electron Wavefunction

In planar barrier structures, such as nanowires, the potential varies only in one dimension - the direction of the vertical growth, in this case chosen to be the z-direction. This means that the electrons are well confined in the x and y-directions and can move freely along the axis of the wire, the z-axis. The states of the electrons in a quantum wire can be described with an envelope function by assuming the effective mass approximation (Ref. [7]),

$$\Psi(\vec{r}) = \psi_k(z)\phi_{n,m}(x,y) \quad , \tag{1}$$

where n and m are the main quantum numbers confining the electron in the x and y directions respectively, and k is the longitudinal momentum of the electron. The transverse part of the wavefunction, $\phi_{n,m}$, satisfies the time-independent Schrödinger equation (SE),

$$\Big[\frac{\hbar^2}{2m^*}\nabla^2 + V_{\text{eff}}(x,y)\Big]\phi_{n,m}(x,y) = E_{n,m}\phi_{n,m}(x,y) \quad , \tag{2}$$

where m^* is the isotropic effective mass, $E_{n,m}$ is the eigenenergy and V_{eff} is the effective potential which includes contributions from the electrostatic potential, the potential of band discontinuities, the average potential of ionised donors and acceptors and a many-body potential contribution due to free charge carriers. The potential is constant in x and y directions and is considered infinite outside the nanowire. In other words, the workfuncion is large compared to the relative electron energies considered here. The potential thus confines the electrons in x and y directions and the solution to Eq. 2 consists of standing waves and its eigenenergies form subbands or channels. Now, if we

consider the wire to have a rectangular cross-section and assume an infinite potential outside the wire as stated earlier, the following solution is obtained, see Ref. [7],

$$\phi_{n,m}(x,y) = \Big(\frac{4}{L_x L_y}\Big)^{1/2} \sin(\frac{n\pi x}{L_x})\sin(\frac{m\pi y}{L_y}) \quad , \tag{3}$$

where L_x and L_y are the dimensions of the wire in x and y directions respectively and n and m take integer values, i.e. $n, m = 1, 2, 3, \ldots$. On the other hand, the z-component of the wavefunction, $\psi_k(z)$, satisfies the following time-independent Schrödinger equation,

$$\Big[\frac{\hbar^2}{2}\frac{\partial}{\partial z}\frac{1}{m^*}\frac{\partial}{\partial z} + V\Big]\psi_k(z) = E_k\psi_k(z) \quad , \tag{4}$$

where V is now assumed to be constant potential forming a barrier and E_k is the electron eigenenergy. This is an ordinary differential equation and yields the following general solution,

$$\psi_k(z) = \frac{1}{\sqrt{L_z}}\big(Ae^{ikz} + Be^{-ikz}\big) \quad , \tag{5}$$

where A and B are the wave amplitudes and L_z is the wire dimension in the z-direction. The total eigenenergy is then found to be,

$$E_{k,n,m} = E_{k_z} + E_{n,m} = \frac{\hbar^2 k^2}{2m^*} + \frac{n^2\hbar^2\pi^2}{2m^* L_x^2} + \frac{m^2\hbar^2\pi^2}{2m^* L_y^2} \quad , \tag{6}$$

where a pair of the quantum numbers n, m describes a continuum of 1D states which can be referred to as a subband, a mode or a channel, see Ref. [7].

3.2 Resonant Tunnelling

Unlike in classical mechanics, quantum particles such as electrons can tunnel through a potential barrier and thus enter a classically forbidden region where the energy of the particle is lower than the potential energy of the barrier itself. Such a phenomenon only occurs if certain boundary conditions at the interface of different media are fulfilled; the wavefunction and its normal derivative divided by the effective mass must be continuous across the boundary separating the two media with different potential energies. The requirement of continuity stems from the fact that a spatially discontinuous solution to the SE would lead to an infinite probability of finding a quantum particle at a particular point, which is physically not possible. As a consequence, the electrons have a certain

probability of transmitting through a potential barrier or being reflected at a boundary. Such scattering at a boundary is described by transmission and reflection coefficients, $T(E)$ and $R(E)$, which depend on the electron energy.

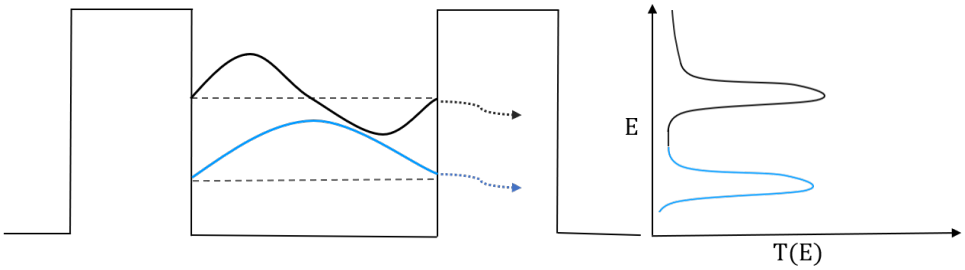

Figure 5: The bound states of a finite potential well with the transmission function $T(E)$ indicated on the right.

When the transmission coefficient, defined as the probability for electrons to tunnel through a barrier structure, is sharply peaked at certain energies we are referring to the *resonant tunnelling*. The resonant energy at which the tunnelling occurs is associated with a bound state with a finite lifetime in the quantum well surrounded by two barriers, as shown in Fig. 5. Then the width of the resonant energy (the energy range in which the transmission coefficient is sizeable) is inversely proportional to the lifetime of the bound state. Depending on the width and the height of the barrier, several such quasi-bound states exist inside the well.

3.3 Transmission Formalism

As electrons tunnel through the barrier structure, a resulting transmission current arises. To compute the current I in a low dimensional device, several assumptions have to be made. In the macroscopic case, the resistance is dependent on the length of the conductor, L, as $R = \frac{L}{W\sigma}$, where σ is the conductivity and W is the area of the conductor. However, as the dimensions of the conductor become smaller, the Ohmic relation breaks down and a certain limiting value of the conductance, defined as $G = \frac{1}{R}$, is approached. The relation between the voltage applied, the current and the conductance on a nanoscale is the key to the current calculations and to the understanding of the different possibilities of improving the efficiency of a nanowire-based solar cell. Ref. [8]

In our model, depicted in Fig. 6, we will assume contact reservoirs on both the left and the right side of the barrier structure connected to the barrier via conducting leads. Since we have a non-equilibrium system, the reservoirs are described by an unknown distribution function f_k, yet to be specified for each reservoir. Furthermore, it is assumed that the contacts (the reservoirs) are perfectly absorbing, meaning that when an electron is transmitted through the barrier structure and reaches the contact reservoir on the other side, it looses all its excess energy and its phase coherence (the memory of its previous state) in the contact.

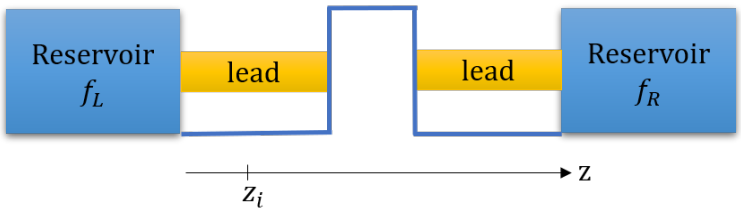

Figure 6: Visualisation of the transmission formalism model.

As mentioned, the Hamiltonian that acts on the electron wavefunction can be separated into longitudinal (z-direction) and transverse ($x-y$ plane) components which facilitates the calculations of the current. As we are only interested in the flow from left to right (z-direction), we can consider only the z-dependent part of the wavefunction. Since probability is a conserved quantity in quantum mechanics, it follows that it obeys the continuity equation which relates the probability flux out of a region and the probability in that region, Ref. [9]. The probability flux in the z-direction, s_z, is defined as

$$s_z = \frac{i\hbar}{2m}\left(\psi\frac{\partial\psi^*}{\partial z} - \psi^*\frac{\psi}{\partial z}\right) = \frac{\hbar k}{mL}. \tag{7}$$

If we now consider the current at a point z_i on the left side of the barrier, the current can be obtained by integrating the current probability flux over all possible k values. When we are summing up over all possible k values, we must also include the occupation of states which weights the likelihood of a certain k state to be occupied. The expression then becomes,

$$I = \frac{L}{2\pi}\int_{-\infty}^{\infty} 2\frac{e\hbar k}{mL} f_k dk \quad , \tag{8}$$

where the 2 in the integral comes from the spin degeneracy and $\frac{1}{2\pi}$ factor appears as the

sum of the momenta is converted into an integral.
Realising the expression for velocity, $v = \frac{\hbar k}{m} = \frac{1}{\hbar}\frac{\partial E}{\partial k}$, in Eq. (8) and dropping the partial derivatives (since we are integrating over one dimension of k only), we can convert the integral and integrate over energy instead. The current measured at a point z_i stems from carriers injected by the left reservoir which are incident on the barrier as well as those that are reflected, having a weighted occupation of states by the reflection coefficient, $R(E)$. The carriers that are injected into the system by the right reservoir can contribute to the current at z_i if they are transmitted through the barrier. Thus the occupation of states of these carriers must be weighted by the transmission coefficient $T(E)$. The expression for current then becomes,

$$I = \frac{2e}{h}\Big(\int_0^\infty f_L(E)T(E)dE - \int_0^\infty f_R(E)T(E)dE\Big) \quad , \tag{9}$$

where $f_L(E)$ and $f_R(E)$ are the distribution functions of the carriers originating in left and right reservoir respectively and the conservation of current, $T(E)+R(E) = 1$, was applied.

In thermal equilibrium, the reservoirs can be described by Fermi distribution functions and by quasi-Fermi potentials μ_L and μ_R of the left and right reservoir respectively. We refer to quasi-Fermi rather than a Fermi level as the electron distribution is displaced from equilibrium and hence the conduction and valence bands have to be each described by its quasi-Fermi potential and no longer by a single Fermi potential. This assumption stems from the fact that the recombination time of the electrons across the band gap is much longer than the relaxation time within respective band. In the low temperature limit, the difference between the distribution functions has the form of a step function and is nonzero only in the interval $\mu_R < E < \mu_L$. This simplifies the expression for current and yields

$$I = \frac{-2e}{h}\int_{\mu_L}^{\mu_R} T(E)dE. \tag{10}$$

If we assume that the applied voltage is small, the energy range of the electrons is narrow and thus the energy dependence of the transmission coefficient $T(E)$ can be neglected.

We then arrive at the expression for current

$$I = \frac{2e}{h} T(\mu_L - \mu_R). \tag{11}$$

The voltage measured across the structure is then $eV = \mu_L - \mu_R$ and the alternative to Ohm's law for low dimensional conductors is

$$\frac{I}{V} = G = \frac{2e^2}{h} T \quad , \tag{12}$$

where $\frac{2e^2}{h}$ is the fundamental conductance.

If we are interested in the current dependence on electron energy, the key quantity which needs to be computed is the transmission coefficient $T(E)$ for a range of energies which can then be referred to as a transmission function, which describes the transmission for a specific barrier structure. Such a transmission function can be computed using the transfer matrix method which is explained in the following section.

3.4 The Transfer Matrix Method

When an electron, described by the wavefunction from Sec. 3.1, approaches a potential barrier, it scatters. As depicted in Fig. 7, an electron travelling from left to right through the barrier system has a certain probability of being reflected or transmitted at the first barrier. In the same manner, the wavefunction transmitted through the first barrier scatters off the following barrier and is again partially reflected and partially transmitted. Unlike from the first scattering, the reflected wavefunction can now interfere with the

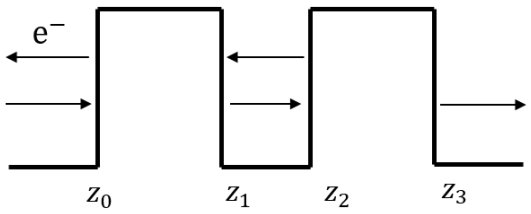

Figure 7: The possible paths of the electron wavefunction.

wavefunction transmitted from the first barrier. Our goal is to relate the amplitudes of the respective wavefunctions at each of the boundary points, z_0, z_1, z_2 and z_3, in order to compute the transmission probability, i.e. the transmission coefficient $T(E)$. This can be

done by applying the transfer matrix theory which uses a so-called scattering matrix or S-matrix to relate the wave amplitudes of the incoming and outgoing waves at a potential boundary. The following description closely follows Ref. [10] and Ref. [11] where the transfer matrix method was applied for similar computations.

Let us consider the z-component of the electron wavefunction on both sides of the boundary at z_0,

$$\psi_L(z) = Ae^{ik_L z} + Be^{-ik_L z} \quad z \leq z_0 \tag{13}$$

$$\psi_R(z) = Ce^{ik_R z} + De^{-ik_R z} \quad z \geq z_0 \quad , \tag{14}$$

where ψ_L and ψ_R describe the electron wavefunctions on the left and right side of the boundary z_0, respectively. The variables k_L and k_R are the electron momenta defined as

$$k_L = \frac{\sqrt{2m_L(E - V_L)}}{\hbar} \quad \text{and} \quad k_R = \frac{\sqrt{2m_R(E - V_R)}}{\hbar} \quad , \tag{15}$$

where V_L and V_R are the potentials on the left and right side of the boundary and thus the momenta can take both real and imaginary values. The wavefunctions must obey the following boundary conditions,

$$\psi_L(z_0) = \psi_R(z_0) \quad \text{and} \quad \frac{1}{m_L}\frac{d\psi_L}{dz}\Big|_{z_0} = \frac{1}{m_R}\frac{d\psi_R}{dz}\Big|_{z_0}, \tag{16}$$

where m_L and m_R are the electron effective masses on the left and right side of the boundary. Eq. (13) and Eq. (14) provide;

$$Ae^{ik_L z_0} + Be^{-ik_L z_0} = Ce^{ik_R z_0} + De^{-ik_R z_0} \tag{17}$$

$$\frac{k_L}{m_L}(Ae^{ik_L z_0} - Be^{-ik_L z_0}) = \frac{k_R}{m_R}(Ce^{ik_R z_0} - De^{-ik_R z_0}). \tag{18}$$

For the case that $z_0 = 0$, the exponential functions simplify to 1 and the amplitudes C and D of the outgoing wave can be expressed in terms of amplitudes A and B of the incident wave by adding and subtracting Eq. (17) and Eq. (18). The resulting system of

equations can be written in a matrix form as follows,

$$\begin{bmatrix} C \\ D \end{bmatrix} = \frac{1}{2m_L k_R} \begin{bmatrix} m_R k_L + m_L k_R & m_L k_R - k_L m_R \\ m_L k_R - k_L m_R & m_L k_R + k_L m_R \end{bmatrix} \begin{bmatrix} A \\ B \end{bmatrix} = M_d \begin{bmatrix} A \\ B \end{bmatrix} \quad , \tag{19}$$

where M_d is sometimes referred to as the discontinuity matrix since it relates the effective masses and the momenta of the electron in the different media surrounding the boundary. In general, one must also consider the case of a nonzero z and include the propagation parts of the wavefunctions when relating the amplitudes. If we write the wavefunctions in a dot product form, we can obtain a matrices which describe the translation of the electron wavefunction on on each side of the boundary,

$$\psi_L(z) = \begin{bmatrix} e^{ik_L z} & e^{-ik_L z} \end{bmatrix} \begin{bmatrix} A \\ B \end{bmatrix} \equiv \begin{bmatrix} e^{ik_L z} & e^{-ik_L z} \end{bmatrix} \Phi_L. \tag{20}$$

If the wavefunction ψ_L is translated by a distance P, we have

$$\psi_L^{'}(z') = \psi_L(z^{'} + P) = \begin{bmatrix} e^{ik_L z} & e^{-ik_L z} \end{bmatrix} \begin{bmatrix} A e^{ik_L P} \\ B e^{-ik_L P} \end{bmatrix} \equiv \begin{bmatrix} e^{ik_L z} & e^{-ik_L z} \end{bmatrix} \Phi_L^{'}. \tag{21}$$

Now Φ_L and $\Phi_L^{'}$ are related by a propagation matrix M_L in the following way

$$\Phi_L^{'} = M_L \Phi_L \quad , \tag{22}$$

where

$$M_L = \begin{bmatrix} e^{ik_L P} & 0 \\ 0 & e^{-ik_L P} \end{bmatrix}. \tag{23}$$

In the same way the propagation matrix for the wavefunction on the right side of the barrier, defined as M_R, can be obtained

$$M_R = \begin{bmatrix} e^{ik_R P} & 0 \\ 0 & e^{-ik_R P} \end{bmatrix}. \tag{24}$$

Combining the discontinuity and propagation matrices of general form (replacing distance P by a variable z), a general expression for the wavefunction amplitudes C and D in terms

of amplitudes A and B can be obtained,

$$\begin{bmatrix} C \\ D \end{bmatrix} = \frac{1}{2m_L k_R} \begin{bmatrix} e^{-ik_R z} & 0 \\ 0 & e^{ik_R z} \end{bmatrix} \begin{bmatrix} m_R k_L + m_L k_R & m_L k_R - k_L m_R \\ m_L k_R - k_L m_R & m_L k_R + k_L m_R \end{bmatrix} \begin{bmatrix} e^{ik_L z} & 0 \\ 0 & e^{-ik_L z} \end{bmatrix} \begin{bmatrix} A \\ B \end{bmatrix}, \tag{25}$$

we define

$$M_S(z) \equiv \frac{1}{2m_L k_R} \begin{bmatrix} e^{-ik_R z} & 0 \\ 0 & e^{ik_R z} \end{bmatrix} \begin{bmatrix} m_R k_L + m_L k_R & m_L k_R - k_L m_R \\ m_L k_R - k_L m_R & m_L k_R + k_L m_R \end{bmatrix} \begin{bmatrix} e^{ik_L z} & 0 \\ 0 & e^{-ik_L z} \end{bmatrix} \tag{26}$$

as the general form of the S-matrix for a boundary at certain position z. Due to the S-matrix being multiplicative, the total transmission through a system of barriers can be described by the product of the S-matrices at each potential boundary, which is defined to be the transfer matrix, also referred to as the T-matrix. The T-matrix for our two barrier system is then the product of the S-matrices of each of the four boundaries,

$$\begin{bmatrix} C \\ D \end{bmatrix} = M_S(z_3) M_S(z_2) M_S(z_1) M_S(z_0) \begin{bmatrix} A \\ B \end{bmatrix} = M_T \begin{bmatrix} A \\ B \end{bmatrix}. \tag{27}$$

As mentioned earlier, we only consider the electron coming from the left towards the barrier system, hence the D amplitude of the wavefunction on the right side of the boundary is set to zero. Similarly, the amplitude A of the wavefunction on the left hand side of the barrier is set to 1 as it describes the incoming wavefunction and the amplitude B is then the amplitude of the reflected wavefunctions and can be renamed to r. The transmitted wave is described by the amplitude C which is denoted by t. Then Eq. (24) can be rewritten as

$$\begin{bmatrix} t \\ 0 \end{bmatrix} = M_T \begin{bmatrix} 1 \\ r \end{bmatrix}. \tag{28}$$

Solving the matrix equation, we find that the transmission amplitude t has the following form,

$$t = \frac{M_{T11} M_{T22} - M_{T21} M_{T12}}{M_{T22}}. \tag{29}$$

The desired transmission coefficient, $T(E)$, of an electron of a specific energy is defined

as the transmission current over the incident current,

$$T(E) = \frac{|\ t\ |^2\ \frac{k_2}{m_2}}{1^2 \frac{k_1}{m_1}} \quad , \tag{30}$$

where k_1 and k_2 are the momenta in the left and right leads and m_1 and m_2 are the effective masses in the left and right leads respectively. In the case of this thesis, the leads are always made out of the same material and thus the expression for the transmission coefficient simplifies to

$$T(E) = |\ t\ |^2 \ . \tag{31}$$

3.5 Simplified Γ and Ω Factors

In order to be able to later explain the behaviour of the transmission function when varying the barrier widths, we need to introduce two new parameters. The transmission through a barrier structure depends on the rates at which electrons enter and leave the structure. These rates are not necessarily the same as they depend on the dimensions of the barriers and wells in the structure. The rate at which electrons flow in/out is defined to be the constant Γ, $\Gamma = \frac{\hbar}{t}$, where t is the average time an electron spends inside the structure. One can visualise the constant as the full width at half maximum (FWHM) of the transmission peaks, in other words the energy resolution of the transmission peaks, which can be mathematically shown by doing a Fourier transform of the time-dependent probability function.

The second factor affecting the transmission, that is considered in this thesis, is the overlap of the wavefunctions which describe the respective bound states in the wells of the multibarrier structure. The size of the overlap is characterised by the tunnelling coupling constant between the wells, defined as Ω. The coupling constant Ω can be perceived as the size of the peak splitting for each of the transmission peaks. For the case of a three barrier structure, the size of the splitting is equivalent to 2Ω as shown in Appendix A1. The size of the peak splitting has a different value depending on the number of barriers/wells involved in the structure. In the case of four barriers, an additional energy state arises resulting in more possible interactions between the wells. Yet the exact size of the splitting in terms of Ω can be obtained by following the same method as in the case of a

three barrier structure in Appendix A1.

The relative size of Ω and Γ then determines the splitting of the transmission peaks. Let us consider a three barrier structure. In the case of the coupling of the wells being smaller than the rate at which the electrons enter/leave the system, the peak splitting vanishes and the transmission probability decreases. This is because the probability for the electrons to appear in the second well is much lower than the probability to find them in the first well (see Appendix A2 for more detail). The small fraction of electrons that transmits through the central barrier has no time to oscillate between the outer barriers as the period of the oscillation is longer than the average time the electrons spend in the structure.

In the case of the coupling of the wells being larger than the escape rate of the electrons, it is equally probable for the electrons to be in either of the wells. Thus, the electrons oscillate in between the outer barriers, resonance occurs and clear splitting of the transmission peaks can be observed.

4 Discussion and Results

Before introducing and commenting on the results, the notation will be clarified. The multi-barrier structures studied are illustrated in Fig. 8 with the respective barrier and well widths indicated. To simplify the referring to the structures, each barrier structure will be specified by a list of the barrier and well widths in the unit of nanometres. For example, for the case of the barrier system in Fig. 8a the list would be $[\mathbf{B_1}, W_1, \mathbf{B_2}, W_2, \mathbf{B_3}]$. When a specified parameter of the barrier structure is varied, it is indicated with an x.

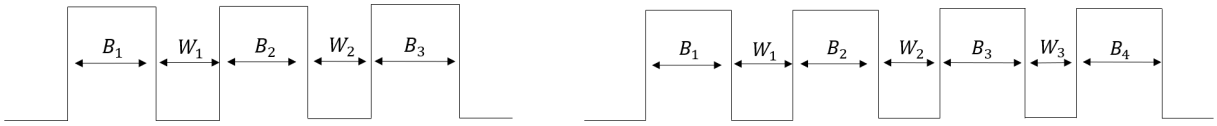

(a) Three barrier filter (b) Four barrier filter

Figure 8: Filters with indicated barrier widths $\mathbf{B_i}$ and well widths W_i where i takes integer values.

As mentioned, the overall aim is to identify a multi-barrier system (with three or four barriers) which maximizes the transmission of electrons with energy range 0.492-0.504 eV and blocks electrons below 0.460 eV and above 0.550 eV.

4.1 Three Barrier Filter

From the energy solution of the time-independent SE, Eq. (6), it is clear that the energies, at which bound states of a potential well appear, decrease with increasing well width as the eigenenergy is inversely proportional to the well width. Such an energy shift of the bound states was also observed during the simulations as depicted in Fig. 9. Hence by changing the well width, the energy spectrum at which the resonance transmission occurs could be chosen. To validate the position of the bound states in the wells and so the position of the transmission resonance peaks, the time-independent SE for a finite quantum well, with a 0.7 eV potential height and a 6.5 nm width, was numerically solved. The bound states found were at 0.115 eV and 0.506 eV, which corresponded to the values obtained for the states in the filter structure considering the offset due to the interaction between the wells. The optimal well width, maximising the transmission in the desired range, was found to be 6.8 nm with bound states approximately at 0.107 eV and 0.502 eV. After identifying the suitable well width for the filter, the widths of the barriers were varied. When increasing the width of the central barrier, the transmission function peaks

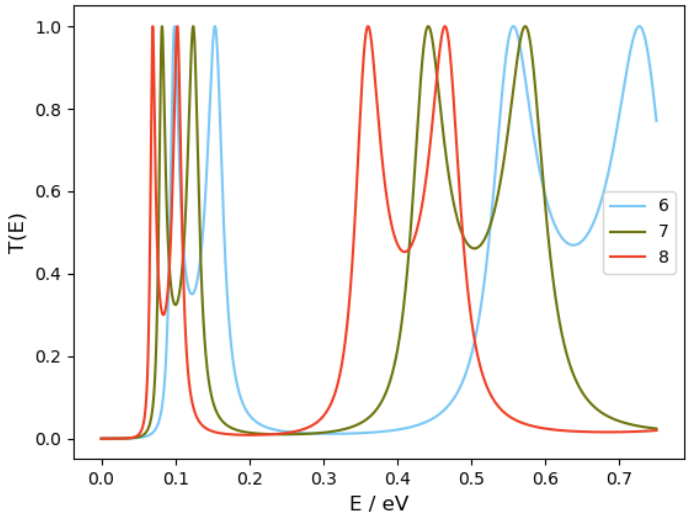

Figure 9: Transmission function for [**1**, x, **1**, x, **1**] structure with varying well widths from 6 to 8 nm.

narrow, the peak splitting vanishes and the transmission probability decreases as shown in Fig. 10a. The lower transmission and the smaller range of resonance energies with greater barrier width is expected from the Ω and Γ coefficients approach explained in Sec. 3.5.

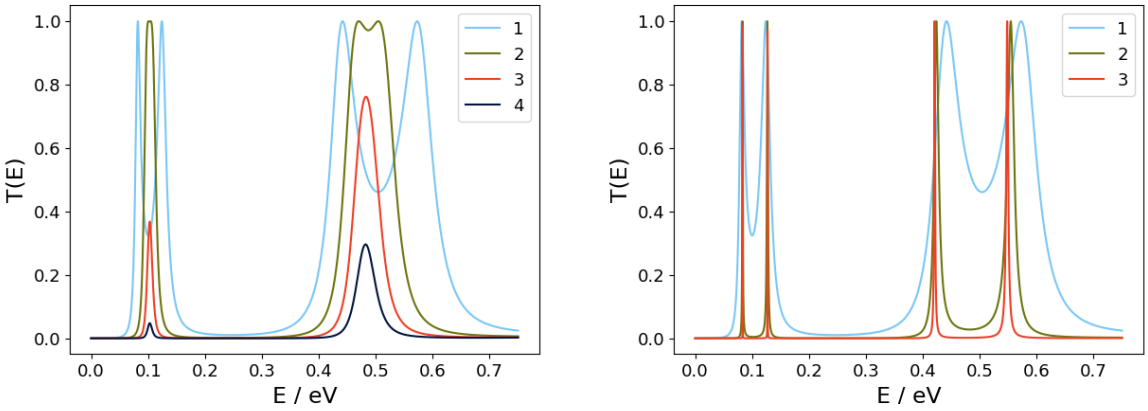

(a) (b)

Figure 10: Transmission function of [**1**, 7, **1**, 7, **1**] structure under variation of the barrier widths, where in (a) the width of the central barrier was varied from 1 to 4 nm and in (b) the width of the outer barriers was varied from 1 to 3 nm

It was observed that the transmission at the second bound state was more favoured when the outer barriers were identical, therefore their width parameters were changed simultaneously. When the width of the outer barriers was increased, the transmission peaks narrowed down more radically than in the case of the inner barrier. This was again foreseen following the explanation of the Ω and Γ coefficients. The values of the coupling coefficients, Ω_1 and Ω_2, for the first and second bound states, were obtained for different barrier structures to confirm the theoretical prediction from Sec. 3.5. This was done by measuring the distance between the split peaks and dividing by 2. When the central barrier was increased, the coupling constants Ω_1 and Ω_2 both decreased (See Tab. 1) as anticipated by the theory in Sec. 3.5. Looking at the values of the coupling constants Ω_1 and Ω_2 in Table. 2, one can conclude that by widening the outer barriers, the resonance energies can be tuned to cover a smaller range or even to reach an exact value of the energy of the bound state.

$\mathbf{B_1}$	$\mathbf{B_2}$	$\mathbf{B_3}$	$\mathbf{\Omega_1}$	$\mathbf{\Omega_2}$
1	1	1	0.042	0.132
1	1.2	1	0.033	0.107
1	1.4	1	0.025	0.086
1	1.6	1	0.018	0.068
1	1.8	1	0.012	0.052
1	2	1	0.004	0.035

Table 1: The variation of the coupling between the two wells as the width of the central barrier is increased, where Ω_1 and Ω_2 are the coupling constants of the first and second bound states respectively.

$\mathbf{B_1}$	$\mathbf{B_2}$	$\mathbf{B_3}$	$\mathbf{\Omega_1}$	$\mathbf{\Omega_2}$
1.2	1	1.2	0.0432	0.133
1.4	1	1.4	0.0435	0.133
1.6	1	1.6	0.0437	0.133
1.8	1	1.8	0.0437	0.131
2	1	2	0.0437	0.131
3	1	3	0.0437	0.127

Table 2: The variation of the coupling between the two wells as the width of the outer barriers is increased, where Ω_1 and Ω_2 are the coupling constants of the first and second bound states respectively.

The width of each barrier was varied from 1 nm to 7 nm keeping the other variables constant. Then different combinations of barriers, for example B_1 and B_2, B_1 and B_3, were varied with barrier widths between 1 to 3 nanometres. After attempting various combinations of barrier widths and identifying the relative transmissions at the first and second state, the most optimal transmission was recorded with a 4 nm wide central barrier and 1 nm wide outer barriers. The transmission function can be seen in Fig. 11.

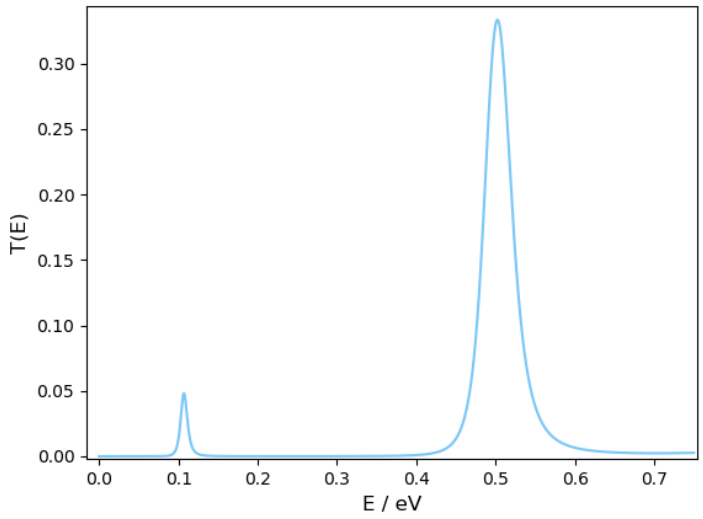

Figure 11: Transmission function for the optimal three barrier system [**1**, 6.8, **4**, 6.8, **1**].

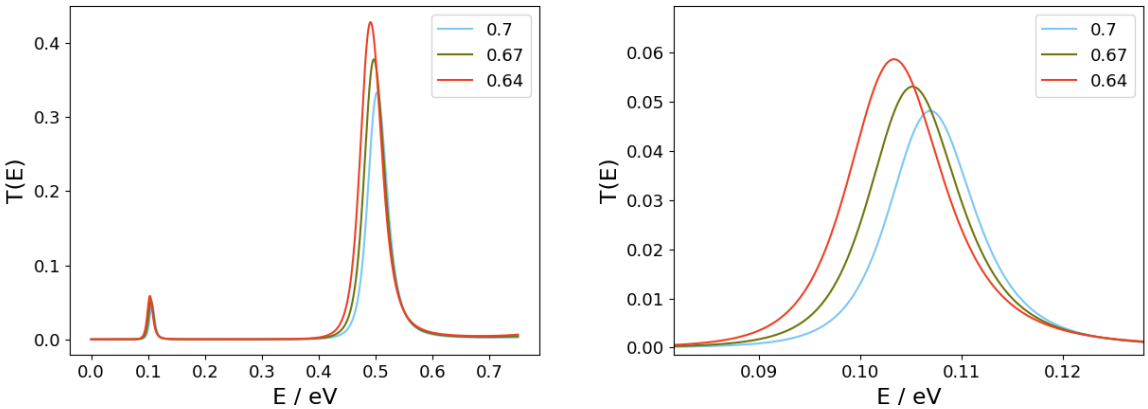

(a) (b)

Figure 12: Validating the reliability of the results by varying the barrier height of a $[\mathbf{1}, 6.8, \mathbf{4}, 6.8, \mathbf{1}]$ structure to 0.7, 0.67 and 0.64 eV in (a), where in (b) the first resonant peak is enlarged.

As mentioned, the offset of the conduction bands is very difficult to measure and no exact value is known. Therefore we had to consider a slight uncertainty in the height of the potential barriers when designing the filter. As shown in Fig. 12, decreasing the potential lowers the bound state energies slightly and increases the transmission probability as could be predicted. Since the shift in energy for a 0.03 eV shift in potential is around 0.005 eV, the variation of the potential should not dramatically affect the effectiveness of the filter.

4.2 Four Barrier Filter

An additional barrier in the filter results in a transmission function with an additional splitting of the resonant peaks as predicted by Ref. [12], where a system of n barriers produces a $(n-1)$-fold splitting of the resonant peaks. Increasing the well widths again shifts down the energies of the bound states as shown in Fig. 13. Unlike in the previous case, higher transmission in the desired energy region, 0.492 eV$< E <$ 0.504 eV, is achieved when a combination of wells with distinct widths is used. When testing different combinations of well widths in the range 6-7 nm (taking steps of 0.1 nm), a particularly satisfying result was obtained for $W_1 = W_2 = 6.3$ nm and $W_3 = 6.8$ nm.

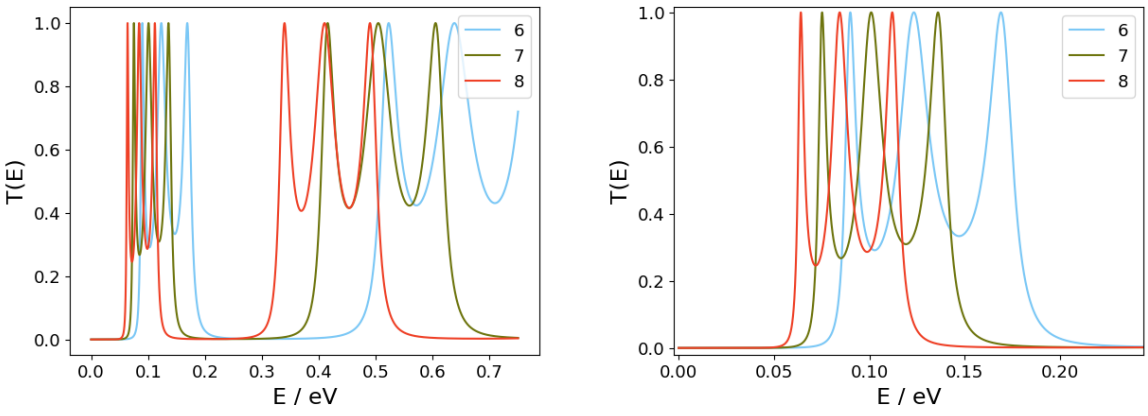

Figure 13: Transmission function for 6, 7 and 8 nm wide wells for a $[\mathbf{1}, x, \mathbf{1}, x, \mathbf{1}, x, \mathbf{1}]$ structure in (a), with the peak at 0.1 eV enlarged in (b).

On the other hand, the behaviour of the transmission function under the variation of the barrier widths is identical to the three barrier case. When varying the widths of the two inner barriers the peaks narrowed down and the peak splitting decreased, while increasing the width of the outer barriers narrowed the peaks more significantly and shifted them

slightly to the lower energies. Such a behaviour of the transmission function, shown in Fig. 14, could be again explained in terms of the Ω and Γ coefficients. Further use of

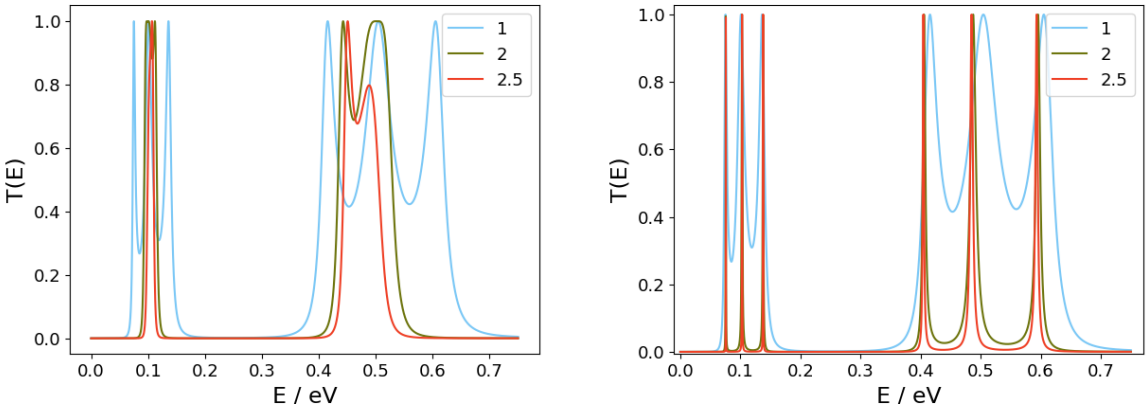

Figure 14: Transmission function of [**1**, 7, **1**, 7, **1**, 7,**1**] structure under variation of the barriers, where in (a) inner barriers, B_2 and B_3, are varied from 1 to 2.5 nm and in (b) the outer barriers, B_1 and B_4, are varied from 1 to 2.5 nm.

asymmetry in the filter design proves to increase the transmission probabilities. When increasing the width of the third barrier, $\mathbf{B_3}$, the transmission is decreased and the peak splitting is suppressed, following the same trend as in the three barrier case, as shown in Fig. 15. Altering the values of $\mathbf{B_2}$ and $\mathbf{B_3}$ between 1-4 nm, both simultaneously and individually, the transmission was the most desirable for $\mathbf{B_2} = \mathbf{1}$ nm and $\mathbf{B_3} = 4$ nm.

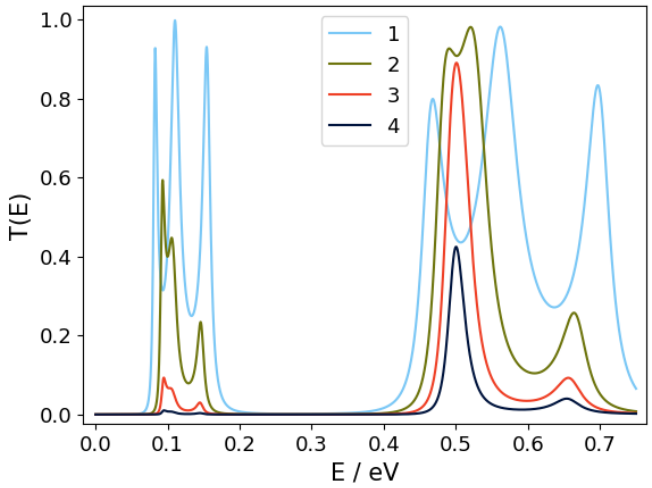

Figure 15: Variation of transmission function for a $[\mathbf{1}, 6.3, \mathbf{1}, 6.3, \mathbf{x}, 6.8, \mathbf{1}]$ structure with the width of the third barrier modified from 1 to 4 nm

The widths $\mathbf{B_1}$ and $\mathbf{B_4}$ were varied in the 1-2 nm range. Like in the case of the inner barriers, they were varied simultaneously as well as separately. As demonstrated in Fig. 16, it was noticed that increasing the barrier width $\mathbf{B_4}$ increases the transmission probability at both resonant energies. It is then the question which factor is more significant

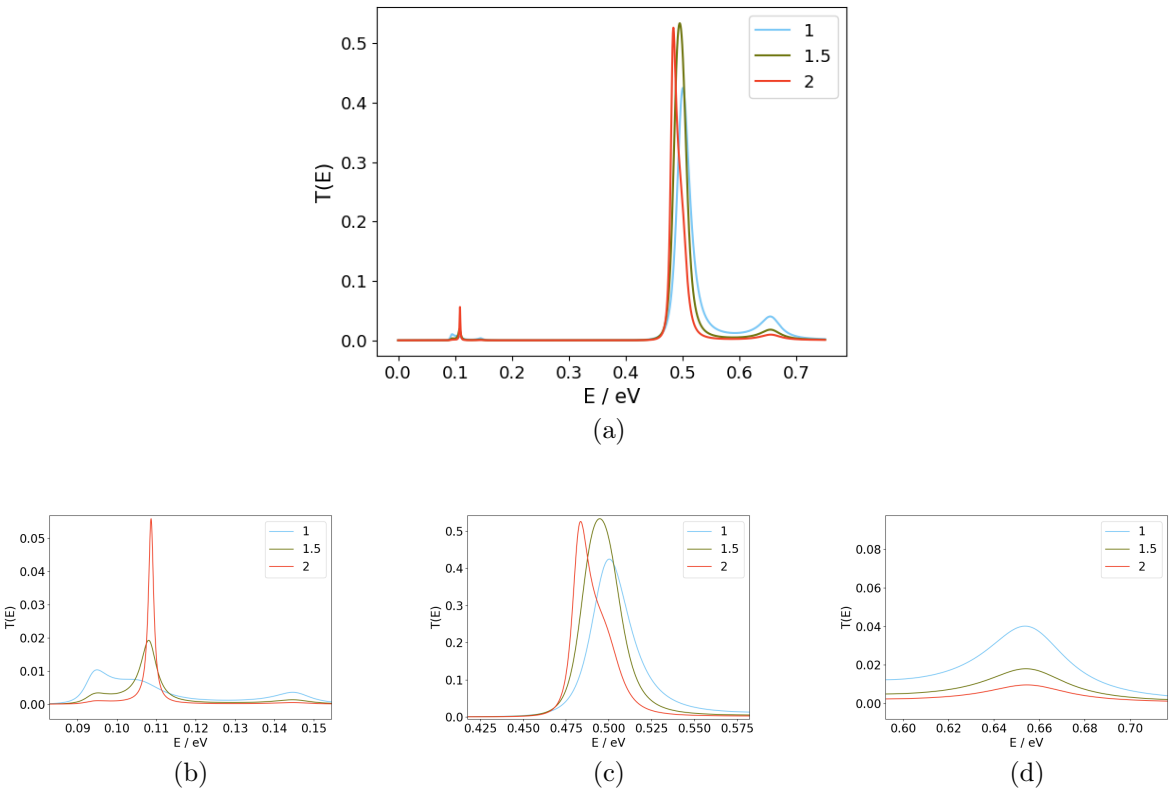

(a) (b) (c) (d)

Figure 16: Variation of the transmission function of the $[\mathbf{1}, 6.3, \mathbf{1}, 6.3, \mathbf{4}, 6.8, \mathbf{x}]$ structure in (a), where the respective peaks are enlarged in (b), (c) and (d).

for a high photocurrent: is it to have the highest possible transmission at the second bound state or to have the lowest possible transmission probability for the first state? The answer is that one must balance both of these factors. However, it is preferred to keep the first bound state resonance peak at very low energies even if it comes with the cost of lowering the transmission at the second bound state. This is because the number of electrons occupying the lower energy state is much higher and thus even with a low transmission probability, the resulting current of these electrons can be quite significant. Weighting these factors, an optimal value for $\mathbf{B_4}$ was found to be 1.4 nm. Varying the barrier widths in any other combinations, i.e. $\mathbf{B_1}$ and $\mathbf{B_2}$ or $\mathbf{B_3}$ and $\mathbf{B_4}$, did not prove to give satisfactory results. Moreover, as for the three barrier filter, the change in the height of the potential barriers did not affect the results significantly. In the case of both the

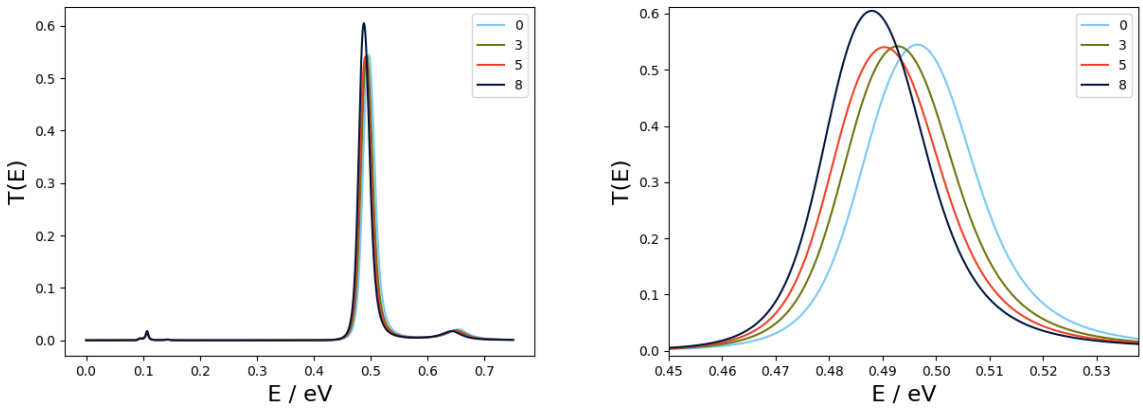

(a) (b)

Figure 17: Trasmission function of the $[\mathbf{1}, 6.3, \mathbf{1}, 6.3, \mathbf{4}, 6.8, \mathbf{1.4}]$ structure where the wells and $\mathbf{B_4}$ include an additional digit, where in b the second peak is enlarged.

three and four barrier filter, the heterostructures can be manufactured with the accuracy of fractions of atoms (on the order of 10^{-11}) by using partially filled layers of InP and InAs. For the filter to preserve its function, the manufacture of the barrier structures can be done with a deviation up to 0.8 Ångström as shown in Fig.17.

5 Outlook

In this thesis, the transmission function for three and four barrier systems was investigated. By varying the well widths of the structure, the bound states were set in order to generate transmission resonant peaks in the desired energy range (0.492-0.504 eV). The variation of the barrier widths changed the peak splitting as well as the peak widths, where the resulting transmission functions could be explained in terms of the Ω and Γ factors. In the three barrier case, a symmetry of the outer barriers and a wider central barrier yielded higher transmissions in the desired range. On the other hand, the four barrier filter gave better results, when asymmetry in both inner and outer barriers was allowed.

Future work could include constructing a distribution function that would describe the occupation of states in the system. This would then allow for the current in the system to be computed facilitating the comparison of the different filter structures.

References

[1] F. H. Alharbi, S. Kais, Renewable and Sustainable Energy Reviews, **43**, 1073, 2015.

[2] J. Nelson, *The Physics of Solar cells*, Imperial College Press, London, 2003.

[3] P. S. Priambodo, N. R. Poespawati and D. Hartanto, *Solar Cells - Silicon Wafer-Based Technologies*, InTech, 2011,
Available from: http://www.intechopen.com/books/solar-cells-silicon-wafer-based-technologies/solar-cell.

[4] J. Rogers, L. Wisland, *Solar Power on the Rise: The Technologies and Policies behind a Booming Energy Sector*, Union of Concerned Scientists, August 2014,
Available from: www.ucsusa.org/solarpowerontherise.

[5] I. Vurgaftman, J. R. Meyer, L. R. Ram-Mohan, *Band parameters for III-V compound semiconductors and their alloys*, Journal of Applied Physics, **89**, 5815, 2001.

[6] M. T. Björk *et al*, *Nanowire resonant tunneling diodes*, Appl. Phys. Lett., **81**, 4458, 2002.

[7] D. K. Ferry, S. M. Goodnick, J. Bird, *Transport in Nanostructures*, 2nd edition, Cambridge University Press, New York, 2009.

[8] S. Datta, *Electronic Transport in Mesoscopic Systems*, Cambridge University Press, New York, 1995.

[9] G. Ohlén, *Phenomena of the quantum world: Theory and concepts*, Department of Physics, Lund University, Lund, 2016.

[10] K. Courteaut, *Modelling of Electron Transport in Thermoelectric Devices Based on Semiconductor Heterostructures*, Bachelor's thesis, Lund University, 2015.

[11] J. S. Walker, J. Gathright, *A transfer-matrix approach to one-dimensional quantum mechanics using Mathematica*, Computers in Physics, **6**, 393, 1992.

[12] R. Tsu, L. Esaki, *Tunneling in a finite superlattice*, Appl. Phys. Lett., **22**, 562, 1973.

A Appendix

A.1 Ω Factor Derivation

Consider a three barrier system where each of the wells has one state, Φ_1 and Φ_2 respectively. The wavefunction that describes a superposition of these states is ;

$$\Psi(z,t) = \Phi_1(z)C_1(t) + \Phi_2(z)C_2(t) \quad , \tag{32}$$

where $C_1(t)$ and $C_2(t)$ are the time-dependent parts of the wavefunction in each of the wells. The electron wavefunction, $\Psi(z,t)$ satisfies the time-dependent SE,

$$i\hbar\frac{\partial}{\partial t}\Psi(z,t) = \hat{H}\Psi(z,t) \tag{33}$$

$$i\hbar\big(\dot{C}_1\Phi_1 + \dot{C}_2\Psi_2\big) = C_1\hat{H}\Phi_1 + C_2\hat{H}\Phi_2 \quad , \tag{34}$$

where the z and t have been dropped in the notation. Multiplying Eq. (34) by $\Phi_1^* \int dz$ and assuming that Φ_1 and Φ_2 are orthogonal, we get

$$i\hbar\dot{C}_1 = C_1\int dz\Phi_1^*\hat{H}\Phi_1 + C_2\int dz\Phi_1^*\hat{H}\Phi_2 \quad , \tag{35}$$

where the first integral is the eigenenergy of the first well, E_1, and the second integral describing the interaction of the two states is defined as Ω. In the same way, when multiplying Eq. (34) by $\Phi_2^* \int dz$, we get

$$i\hbar\dot{C}_2 = C_1\int dz\Phi_2^*\hat{H}\Phi_1 + C_2\int dz\Phi_2^*\hat{H}\Phi_2 \quad , \tag{36}$$

where the first integral is Ω^* and the second one is the eigenenergy of the second well, E_2.

Assuming the two wells are identical ($E_1 = E_2$) and Ω is real, Eq. (35) and Eq. (36) combine to give a matrix differential equation,

$$\begin{bmatrix}\dot{C}_1\\ \dot{C}_2\end{bmatrix} = \frac{1}{i\hbar}\begin{bmatrix}E_1 & \Omega\\ \Omega & E_1\end{bmatrix}\begin{bmatrix}C_1\\ C_2\end{bmatrix} \quad , \tag{37}$$

which can be solved following the general method of finding the eigenvalues and the

eigenvectors and applying the initial conditions

$$C_1(0) = 1 \quad \text{and} \quad C_2(0) = 0. \tag{38}$$

The eigenvalues are obtained by solving the equation,

$$\det \begin{bmatrix} \frac{E_1-\lambda}{i\hbar} & \frac{\Omega}{i\hbar} \\ \frac{\Omega}{i\hbar} & \frac{E_1-\lambda}{i\hbar} \end{bmatrix} = 0 \quad , \tag{39}$$

which yields the following expression for the eigenvalues,

$$\lambda = \frac{1}{i\hbar}\big(E_1 \pm \Omega\big). \tag{40}$$

Here we see that the range of the energies at which transmission occurs is between $E_1 + \Omega$ and $E_1 - \Omega$. The distance between the split transmission peaks is hence precisely 2Ω. Coming back to the dependence of the splitting on the barrier thickness, the resonance energy range clearly depends on the value of Ω. For a wide central barrier, the states Φ_1 and Φ_2 of the two wells can communicate less and thus Ω has a lower value, so low that it is lower than the the constant Γ. Then the distance between the split peaks, 2Ω is very small and hence a single peak without splitting is observed when the transmission function is plotted.

To find the eigenvectors of the form $\begin{bmatrix} \alpha \\ \beta \end{bmatrix}$, we now have to solve the following matrix equation for each of the eigenvalues,

$$\frac{1}{i\hbar} \begin{bmatrix} E_1 & \Omega \\ \Omega & E_1 \end{bmatrix} \begin{bmatrix} \alpha \\ \beta \end{bmatrix} = \frac{E_1 \pm \Omega}{i\hbar} \begin{bmatrix} \alpha \\ \beta \end{bmatrix}. \tag{41}$$

The eigenvectors obtained are $\begin{bmatrix} 1 \\ 1 \end{bmatrix}$ and $\begin{bmatrix} 1 \\ -1 \end{bmatrix}$ for the $\frac{E_1+\Omega}{i\hbar}$ and $\frac{E_1-\Omega}{i\hbar}$ eigenvalues respectively. The general solution can be written as,

$$\begin{bmatrix} 1 & 1 \\ 1 & -1 \end{bmatrix} \begin{bmatrix} Ae^{(E_1+\Omega)t/i\hbar} \\ Be^{(E_1-\Omega)t/i\hbar} \end{bmatrix} = \begin{bmatrix} C_1 \\ C_2 \end{bmatrix} \quad , \tag{42}$$

which leads to the expressions for time-dependent parts, C_1 and C_2, of the wavefunction;

$$C_1 = e^{E_1 t/i\hbar}\Big(Ae^{\Omega t/i\hbar} + Be^{-\Omega t/i\hbar}\Big) \tag{43}$$

$$C_2 = e^{E_1 t/i\hbar}\Big(Ae^{\Omega t/i\hbar} - Be^{-\Omega t/i\hbar}\Big). \tag{44}$$

Applying the initial conditions (See Eq. 38), the coefficients are found to be $A = \frac{1}{2}$ and $B = \frac{1}{2}$. Now it is evident that the two sought functions can be written in terms of sine and cosine,

$$C_1 = e^{E_1 t/i\hbar} \cdot \frac{e^{\Omega t/i\hbar} + e^{-\Omega t/i\hbar}}{2} = e^{E_1 t/i\hbar} \cdot \cos\Big(\frac{\Omega t}{\hbar}\Big) \tag{45}$$

$$C_2 = e^{E_1 t/i\hbar} \cdot \frac{e^{\Omega t/i\hbar} - e^{-\Omega t/i\hbar}}{2} = e^{E_1 t/i\hbar} \cdot i\sin\Big(\frac{\Omega t}{\hbar}\Big). \tag{46}$$

These functions then describe the oscillations of the electrons between the bath and the barrier structure, which can be seen more clearly in Fig. 18 in the following section.

A.2 The Relation between Ω and Γ

To relate the Ω coefficient to the rate at which electrons enter/leave the barrier structure Γ, we plot the probabilities, $|\ C_1\ |^2$ or $|\ C_2\ |^2$, of the electron to be found in the C_1 and C_2 state. As shown in Fig. 18, the probability of an electron to transmit through the barrier

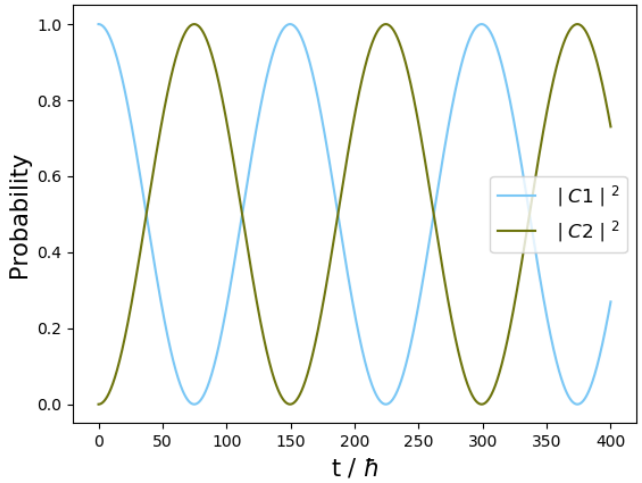

Figure 18: The probability of the electron to be in the C_1 and C_2 state as a function of t/$\hbar$.

and to appear in the second well goes like $\sin^2\left(\frac{\Omega}{\Gamma}\right)$, where the definition of Γ, $\Gamma = \frac{\hbar}{t}$, was applied.

When $\Omega > \Gamma$, which is true at given times, the probability follows the general trend, i.e. the electrons are equally likely to be found in the first and second well, and the electrons oscillate in the structure. However in the case of $\Omega < \Gamma$, the argument of the function becomes small and hence $\sin^2(\frac{\Omega}{\Gamma}) \sim \frac{\Omega^2}{\Gamma^2}$. The probability now follows a quadratic relation and the likelihood of the electron to appear in the second well is significantly suppressed thus no oscillation occurs.

A.3 Python script

```
import matplotlib.pyplot as plt
import numpy as np
import scipy as sc


##############################Defining constants#################################
conversion=3.622626#=sqrt(m_e*eV)/hbar, units:1/nm

# ================================================================================
# ####################Input values defining the barrier system###################
# ================================================================================
#list of values of the potential in the structure
V=[0,0.7,0,0.7,0,0.7,0]
#list of widths in nm, starting with the well  width
L=[1,6.8,4,6.8,1]
#list of effective electron masses in the structure, units: m_e
m=[0.026,0.0795,0.026,0.0795,0.026,0.0795,0.026]
#getting boundary points, i.e. interface of barrier with a well
Z=[0]*(len(V)-1)
for i in range (1,len(Z)):
    Z[i]=Z[i-1]+L[i-1]
# ================================================================================
# ##############################Main method#######################################
# ================================================================================

# # #computing s-matrix for one boundary

def get_s_matrix(z,V_l,V_r,m_l,m_r,E):

    if abs(E-V_r)<1e-6:#considering the case where V_r=E -> k_r=0
            S_1=get_s_matrix(z,V_l,V_r,m_l,m_r,E+1e-3)
            S_2=get_s_matrix(z,V_l,V_r,m_l,m_r,E-1e-3)
            S=0.5*(S_1+S_2)
    else:
        k_l=(sc.sqrt(2*m_l*(E-V_l)))*conversion
        k_r=(sc.sqrt(2*m_r*(E-V_r)))*conversion

        P_1=np.array([[sc.exp(-1j*k_r*z),0],[0,sc.exp(1j*k_r*z)]])
        P_2=np.array([[sc.exp(1j*k_l*z),0],[0,sc.exp(-1j*k_l*z)]])
        D=np.array([[m_r*k_l+m_l*k_r,m_l*k_r-m_r*k_l],[m_l*k_r-m_r*k_l,m_l*k_r+m_r*k_l]])
        P1_D=np.matmul(P_1,D)
        P1DP2=np.matmul(P1_D,P_2)
        S=(1/(2*m_l*k_r))*P1DP2

    return S

# #computing the T-matrix for the heterostructure

def get_t_matrix(Z,V,m,E):
    T=np.array([[1,0],[0,1]])
    for i in range(1,len(Z)+1):
        S_i=get_s_matrix(Z[i-1],V[i-1],V[i],m[i-1],m[i],E)
        T=np.matmul(S_i,T)
    return T



   # #computing the transmission probability for the heterostructure

   def T_prob(T,E):
       k_1=(sc.sqrt(2*m[0]*(E-V[0])))*conversion
       k_2=(sc.sqrt(2*m[len(m)-1]*(E-V[len(V)-1])))*conversion
       t=T[0,0]-(T[1,0]*T[0,1])/T[1,1]
       G=(k_2/m[len(m)-1])/(k_1/m[0])
       T_p=G*abs(t)**2
       return (T_p)

   # ================================================================================
   # ######################Calling functions & Plotting##############################
   # ================================================================================
   #generating list of possible electron energies
   L_E=np.linspace(0.0,0.69,25000)
   #list of the transmission probabilities
   L_T1=[]
   # #generating a list of transmission coefficients for each energy value in L_E
   for i in range (0,len(L_E)):
       L_T1.append(T_prob(get_t_matrix(Z,V,m,L_E[i]),L_E[i]))

   # #plotting the Transmission function
   plt.plot(L_E,L_T1,color='xkcd:lightblue')
   plt.xlabel('E / eV',fontsize=15)
   plt.ylabel('T(E)',fontsize=15)
```